1. Manuscript Title

Glial Contribution to the Pathogenesis of Post-Operative Delirium Revealed by Multi-omic Analysis of Brain Tissue from Neurosurgery Patients

2. Authors names and Affiliations

Takaya Ishii[1, 2, 14], Tao Wang[3], Kazuki Shibata[1, 4], Shota Nishitani[1], Takehiko Yamanashi[5], Nadia E. Wahba[6], Tomoteru Seki[1, 7], Kaitlyn J. Thompson[8], Kyosuke Yamanishi[1, 9], Tsuyoshi Nishiguchi[1, 5], Akiyoshi Shimura[1, 7], Bun Aoyama[1, 10], Nipun Gorantla[1], Nathan J. Phuong[1], Hieu D. Nguyen[1], Therese A. Santiago[1], Yoshitaka Nishizawa [11], Takaaki Nagao[12], Mathew A Howard III[13], Hiroto Kawasaki[13], Kyosuke Hino[2, 14], Atsushi Ikeda[2, 14], Michael P. Snyder[3], Gen Shinozaki[1, 15, *]

[1] Department of Psychiatry and Behavioral Sciences, Stanford University School of Medicine, Palo Alto, California, USA.

[2] Regenerative & Cellular Medicine Kobe Center, Sumitomo Pharma Co., Ltd., Osaka, Osaka, Japan

[3] Department of Genetics, Stanford University School of Medicine, Stanford, CA, USA.

[4] Drug Research Division, Sumitomo Pharma Co., Ltd., Osaka, Osaka, Japan

[5] Faculty of Medicine, Department of Neuropsychiatry, Tottori University, Yonago, Tottori, Japan.

[6] Department of Psychiatry, Oregon Health and Science University, School of Medicine, Portland, Oregon, USA.

[7] Department of Psychiatry, Tokyo Medical University, Shinjuku-ku, Tokyo, Japan.

[8] University of Nebraska Medical Center, Omaha, Nebraska, USA

[9] Department of Neuropsychiatry, School of Medicine, Hyogo Medical University, Nishinomiya, Hyogo, Japan.

[10] Department of Anesthesiology and Intensive Care Medicine, Kochi Medical School, Kochi, Kochi, Japan

[11] Department of Psychiatry, Osaka Medical and Pharmaceutical University School of Medicine, Osaka, Japan.

[12] Department of Neurosurgery (Sakura), Toho University School of Medicine Faculty of Medicine, Sakura, Chiba, Japan

[13] Department of Neurosurgery, University of Iowa Carver College of Medicine, Iowa City, IA, USA

[14] Current affiliation is RACTHERA Co., Ltd., Kobe, Hyogo, Japan

[15] Department of Psychiatry, University of Iowa Carver College of Medicine, Iowa City, Iowa, USA

*Corresponding author: Gen Shinozaki, MD. E-mail: gens@stanford.edu

3. Author contributions

TI: Research design, Data processing, Data analysis, Visualization, and Writing the initial draft and final edit of the manuscript; TW: Data analysis and Writing the initial draft of the manuscript; KS, TY: Conducting experiments; SN, TS: Data processing and Writing the initial draft of the manuscript; NEW, KJT: Collection of clinical data and Data analysis; KY, T Nishiguchi, AS, BA, NG, NJP, HDN, TAS, KH, AI: Critical review of the manuscript; T Nagao: Collecting and processing samples; MAH, HK: Research design support and Collecting samples; MPS: Research design and Final edit of the manuscript; GS: Conceptualization, Research design and Writing the initial draft and final edit of the manuscript

4. Conflict of Interest

TI, KH, and AI are employees of Sumitomo Pharma Co., Ltd. and are currently affiliated with RACTHERA Co., Ltd. GS has pending patents as follows: “Epigenetic Biomarker of Delirium Risk” in the PCT Application No. PCT/US19/51276, in the PCT Application No. PCT/US21/63166 and in U.S. Provisional Patent No. 62/731599; “Non-invasive device for predicting and screening delirium” in the PCT application no. PCT/US2016/064937 and in US provisional patent no. 62/263,325; “Prediction of patient outcomes with a novel electroencephalography device,” in US provisional patent no. 62/829,411; “DEVICES, SYSTEMS, AND METHOD FOR QUANTIFYING NEURO-INFLAMMATION” in the US Patent Application No. 63/124,524. MPS is a cofounder and scientific advisor of Crosshair Therapeutics, Exposomics, Filtricine, Fodsel, iollo, InVu Health, January AI, Marble Therapeutics, Mirvie, Next Thought AI, Orange Street Ventures, Personalis, Protos Biologics, Qbio, RTHM, SensOmics. MPS is a scientific advisor of Abbratech, Applied Cognition, Enovone, Jupiter Therapeutics, M3 Helium, Mitrix, Neuvivo, Onza, Sigil Biosciences, TranscribeGlass, WndrHLTH, Yuvan Research. MPS is a

cofounder of NiMo Therapeutics. MPS is an investor and scientific advisor of R42 and Swaza. MPS is an investor in Repair Biotechnologies. All other authors declare no conflict of interest.

5. Funding Sources

Gen Shinozaki received funding from NIH (MH119165, AG084710) and Sumitomo Pharma Co., Ltd.

Sponsors did not influence the study design and interpretation of the results.

Abstract

Post-operative delirium (POD) is a common complication after surgery especially in elderly patients, characterized by acute disturbances in consciousness and cognition, which negatively impacts long-term outcomes. Effective treatments remain elusive due to the unclear pathophysiology of POD. To address the knowledge gap, we investigated DNA methylation profiles and gene expression changes in brain cells from POD and non-POD patients who underwent brain resection surgery for medication refractory epilepsy. DNA methylation analysis revealed alteration in epigenetic status of immune and inflammation-related genes. Single-nucleus RNA sequencing (snRNAseq) identified POD-specific glial cell alterations, particularly in microglia, where neuroinflammation was strongly enhanced, consistent with epigenetic findings. Astrocytes exhibited changes in synapse-related functions and migration. Furthermore, downstream analysis indicated similarities between POD-associated glial cell states and pathologies such as encephalitis and dementia. Overall, this study—the first multi-omics analysis of brain tissue from POD patients—provides direct evidence of glial cell contributions to POD pathogenesis, and highlights potential therapeutic targets.

Introduction

Delirium is a severe neuropsychiatric syndrome characterized by acute impairments in attention and cognition. Among its various subtypes, Post-Operative Delirium (POD) is particularly prevalent in elderly patients following surgery and is associated with increased mortality, prolonged hospitalization, and long-term cognitive decline[1–3]. Despite its clinical significance, the pathophysiological mechanism of POD remains largely unknown, hindering the development of effective preventive and therapeutic strategies. Identifying reliable biomarkers for POD is crucial for improving patient outcomes and also advancing our understanding of its underlying mechanisms.

Epigenetic modifications, particularly DNA methylation changes, have emerged as potential biomarkers for delirium. Our previous studies demonstrated consistent patterns of alterations in DNA methylation levels in blood cells among delirium patients. This was replicated across four independent cohorts[4]. However, the extent to which these changes in peripheral tissues correlate with molecular alterations in the brain remains unclear. Thus, a direct investigation of brain tissue is essential for elucidating the neurobiological mechanisms of POD. In a previous study, we compared DNA methylation profiles across brain, saliva, and blood samples from medication-refractory epilepsy patients undergoing brain resection surgery, stratified by the presence or absence of POD [5]. While inflammatory signatures potentially linked to delirium were detected in both the brain and blood, their molecular profiles showed limited overlap, underscoring the need for a more detailed analysis of brain tissue. However, studies examining delirium-specific changes in the brain remain scarce due to the difficulty of obtaining brain samples, leaving fundamental aspects of its pathogenesis unexplored.

Single-cell and single-nucleus RNA sequencing (scRNAseq/snRNAseq) provide powerful tools for characterizing the transcriptomic landscape of individual brain cells. These techniques have been widely applied in neurodegenerative and psychiatric disorders[6,7], offering new insights into pathophysiology, biomarker discovery, and therapeutic targets. While a recent study identified potential POD biomarkers in blood cells using scRNAseq[8], no research to date has employed this approach to analyze brain tissue in POD patients.

In this study, we employ a multi-omics approach (genome-wide DNA methylation analysis and snRNAseq) to identify delirium-specific molecular signatures in brain tissue. By analyzing brain samples, we aim to uncover the epigenetic and transcriptomic features unique to POD, offering new mechanistic insights into its pathophysiology. This study represents the first

application of snRNAseq to human brain tissue in POD, providing a crucial step toward identifying the molecular underpinnings of its pathophysiological mechanisms, leading to the potential therapeutic targets for this serious condition.

Materials and Methods

Subject

DNA methylation data and samples derived from a previous cohort study were analyzed [5,9]. In this cohort, subjects with medication-refractory epilepsy scheduled for brain resection surgery were recruited at the University of Iowa Hospitals and Clinics. This cohort study was approved by the University of Iowa's Human Subjects Research Institutional Review Board (#200112047 and #20190791). The present study was also approved by the Stanford University Institutional Review Board (#62033). All patients underwent a series of two neurosurgical procedures: electrode placement for the identification of seizure focus and subsequent tissue resection. To identify POD cases, detailed chart reviews of medical records including physical, neurological, and mental status as well as nursing reports were conducted. Patients with post-operative fluctuations in awareness and orientation were considered as positive cases of POD. A board-certified consultation liaison psychiatrist (G.S.) reviewed the cases in question for the final decision on delirium categorization [5,10].

For this study, 18 cases were selected for analysis and divided into the POD group and the non-POD group. The 9 cases that developed POD after the brain resection surgery were considered the POD group, and the 9 cases that did not develop POD after both surgeries were considered the non-POD group. **Table 1** describes the detailed characteristics of the subjects.

Brain sample collection and processing

Brain samples were immediately stored at -80°C, i.e., flash-freezing, after brain resection. For snRNAseq analysis, nuclei were isolated from the frozen tissues as previously described [11]. Briefly, frozen tissue was homogenized in a chilled lysis buffer using a Dounce homogenizer, followed by differential centrifugation with iodixanol gradient separation to isolate the nuclei. The nuclei pellet was then carefully collected, resuspended, and subjected to additional washes and centrifugation steps. The final nuclei were resuspended in PBS/1% BSA, and utilized for further analysis. For DNA methylation analysis, genomic DNA was extracted from bulk samples using the MasterPure DNA extraction kit (Epicentre) as described in previous publications [5].

DNA methylation analysis

DNA derived from brain tissues was bisulfite-converted with the EZ DNA Methylation Kit (Zymo Research). Genome-wide DNA methylation was analyzed using the Infinium HumanMethylationEPIC BeadChip Kit (Illumina). The arrays were scanned with the Illumina iScan platform. Raw methylation data was processed on R software[12] using the R packages "ChAMP"[13,14] and "Minfi"[15,16]. Probes were excluded if (i) the detection *p*-value exceeded 0.01, (ii) fewer than three beads were present in at least 5% of samples per probe, (iii) the probes were non-CpG, SNP-related, or multi-hit, or (iv) the probes were located on the X or Y chromosomes. Normalization was performed using beta-mixture quantile dilation[17]. To remove chip batch effects, we used champ.runCombat with protecting group from the removal process. The R package "Rnbeads"[18] employing the limma method[19] was used to perform differential methylation analysis. Age, sex, time under anesthesia, blood loss, smoking status, and alcohol use were included as covariates in the analysis.

snRNAseq sequencing library preparation

10,000 nuclei were applied for library preparation using Chromium Next GEM Single Cell Multiome Reagent Kit (10x Genomics) following the manufacturer's protocol. The libraries were pooled and sequenced in the Illumina NovaSeq PE150 system targeting an average of 50,000 reads per nucleus.

snRNAseq data processing and integration

The raw reads were mapped to human reference genome version GRCh38 and unique molecular identifiers (UMIs) counts for each gene in each cell by CellRanger Arch v2.0.0. (10x Genomics). We used the R(v4.3.2) package Seurat (v.5.0.2)[20] for processing the raw count matrices. Only genes expressed in at least 3 nuclei were considered. For each sample, nuclei were excluded if (i) presented unique genes were fewer than 200 or more than 6,000, or (ii) total UMI counts were less than 500 or over 25,000, or (iii) mitochondrial RNA content was superior to 5%. The individual Seurat objects for each sample were lognormalized using the Seurat function "NormalizeData" with 2,000 variable genes. Then, all samples were integrated by the following functions, "SelectIntegrationFeatures", "PrepSCTIntegration", "FindIntegrationAnchors" and "IntegrateData".

snRNAseq data analysis

Integrated data were utilized for downstream analysis. Age, gender, and mitochondrial content were regressed during the data scaling process. Dimensionality reduction was performed using Principal Component Analysis (PCA) and Uniform Manifold Approximation and Projection (UMAP), incorporating the top 20 principal components (PCs). Cell clusters were identified using the "FindClusters" function. Each cluster was annotated with cell types based on representative marker genes corresponding to major brain cell types, including microglia, astrocytes, oligodendrocytes, oligodendrocyte progenitor cells (OPCs), endothelial cells, excitatory neurons, and inhibitory neurons [21–23]. Clusters expressing markers of multiple cell types were identified as multiplets and excluded. For cell type-specific analysis, clusters corresponding to each cell type were independently extracted and subjected to scaling, dimensional reduction, and clustering in the same manner. Differential gene expression (DEG) analysis was performed with the “Findmarkers” function. In this study, genes meeting the following criteria were defined as DEGs: adjusted p-value < 0.05, Log2 Fold Change > 0.25, and pct > 0.1 (That means that the gene is expressed in more than 10% of cells in at least one of the two groups (POD and non-POD group) being compared). Trajectory analysis was performed using the “monocle3” package [24–27].

Gene Ontology (GO) and pathway analysis

GO analysis for enriched genes in snRNAseq analysis was performed using Metascape (v3.5 20240901) [28], and pathway analysis was performed with QIAGEN Ingenuity Pathway Analysis (IPA) (Version 127006219, Build: ing_ruby). As for DNA methylation data analysis, R package missMethyl [29] was used for GO and pathway analysis by adjusting for the variable number of CpG sites tested in each gene.

Statistical analysis

Most statistical analyses were performed using R software. Regarding enrichment analysis for snRNAseq, p-values were calculated by each platform (Metascape and IPA).

Results

Participant demographics

A total of 18 patients (9 POD, 9 non-POD) who underwent brain resection neurosurgery were analyzed. There was no significant difference between the POD and the non-POD groups in each baseline characteristic **(Table 1)**. Brain samples were taken from various brain regions, including the temporal cortex, frontal cortex, hippocampus, amygdala, and occipital lobe depending on the location of seizure focus.

DNA methylation analysis

DNA methylation analysis at 700,284 CpG sites was determined using the EPIC Infinium Bead as depicted in **Figure 1A**. DNA methylation status was compared between the POD and non-POD groups and ranked by significance based on ascending p-values **(Table S1)**. Even the most significantly different site; cg18199231[*GTF2IRD1*] did not reach statistical significance after p-value adjustment correcting for genome-wide multiple comparison. Given the absence of genome-wide significant signals, we proceeded with further analysis, focusing on CpGs with relatively large changes. In this analysis, differentially methylated CpGs (DMCs) were defined based on criteria referenced from the previous study[30], as CpGs with a p-value < 0.05 and a methylation difference (delta beta-value) > 4% between the two groups. 3,774 DMCs were identified **(Figure 1B)**. PCA plot **(Figure 1C)** and hierarchical clustering heatmap **(Figure 1D)** based on the DMCs demonstrated a clear separation between most POD and non-POD subjects. While the CpG context and gene region distribution of DMCs resembled that of all CpGs **(Figure S1 A, B)**, their methylation rate distribution differed **(Figure 1E)**. Notably, the changes in DNA methylation levels between the non-POD and POD groups varied depending on the initial DNA methylation levels in the non-POD group **(Figure 1F, G)**. Most low-methylated DMCs showed increased DNA methylation in the POD group, whereas high-methylated DMCs displayed both hypermethylation and hypomethylation, with demethylation being more common. Furthermore, high-methylated DMCs contained fewer island-related regions **(Figure S1C)** and transcription start site (TSS) neighbors **(Fig S1E)**, whereas low-methylated DMCs were more frequently associated with island-related regions **(Fig S1D)** and TSS neighbors **(Fig S1F)**.

To assess whether the observed methylation pattern differences contribute to variations in associated gene groups, we performed Gene Ontology (GO) and pathway analyses. Although no GO terms reached statistical significance after FDR correction, several immune-related terms, including T cell differentiation and T cell activation, were ranked among the top ($p < 0.01$), alongside terms related to cell adhesion. Similarly, pathway analysis identified immune-related

pathways, such as the chemokine signaling pathway and human cytomegalovirus infection, as top-ranking **(Table 2)**. Since aging is a major risk factor for POD, we further examined the methylation status of age-associated CpGs. In a recent large-scale study analyzing over 10,000 human samples (manuscript in preparation), we identified 24,744 CpGs with genome-wide significant ($p < 5.78 \times 10^{-8}$) and strong ($R^2 > 0.5$) age-associated methylation changes. Among these, 152 overlapped with the identified DMCs in the present study. Although no GO or pathway terms reached FDR significance in the analysis of *age-associated DMCs*, immune- and inflammation-related terms were among the top-ranked **(Table 3)**. These findings suggest that neuroinflammatory alterations are a key feature of the POD group.

To assess whether these trends were influenced by the original methylation rate and its pattern of change, we analyzed DMCs based on their initial methylation status. Among low-methylated DMCs that exhibited increased methylation in the POD group (1,411 CpGs), the top two GO terms were associated with embryonic skeletal system development, which were also enriched in the analysis of all DMCs. Developmental processes were prominently ranked among the top terms. Although no pathways reached statistical significance, several overlapped with those identified in the analysis of all DMCs, including the Rap1 signaling pathway, insulin signaling pathway, and oxytocin signaling pathway **(Table 4)**. In contrast, GO and pathway analyses of highly methylated DMCs that underwent demethylation in the POD group (906 CpGs) revealed a distinct trend. GO analysis showed that most top-ranking biological process terms were related to immunity and inflammation, with "adaptive immune response" approaching statistical significance (FDR = 0.0595). A similar pattern was observed in pathway analysis, where immune- and inflammation-related pathways were predominant, including the NF-kappa B signaling pathway, which reached statistical significance **(Table 5)**. These findings suggest that enhanced demethylation of highly methylated CpG sites in immune- and inflammation-related genes is a hallmark of the POD group, indicating that neuroinflammatory changes in POD may be epigenetically regulated.

snRNAseq analysis

Although DNA methylation analysis identified unique characteristics associated with POD, the data represented a mixture of multiple cell types from bulk brain tissues. To investigate POD-related changes at the single-cell level, we performed snRNA-seq analysis using brain tissues from the same subjects. Nuclei were isolated from frozen resected brain tissue of the same 18 subjects,

followed by snRNA-seq analysis **(Figure 2A)**. After quality control filtering and clustering (see Methods), we retained 95,017 nuclei, which were categorized into seven distinct cell-type clusters based on the expression of representative marker genes **(Figure 2B, C)**. While the distribution of each cell type varied across samples, all 18 subjects contributed a certain number of nuclei for analysis across all identified cell types and each cell type was present in a consistent proportion in both non-POD and POD groups **(Figure 2D, E)**.

Transcriptional profiling of microglia reveals the upregulation of neuroinflammation in the POD group

Glial cells have been reported to play a crucial role in the pathogenesis of POD through neuroinflammation and other mechanisms[31] ,and our DNA methylation analysis suggests that neuroinflammation may be exacerbated in the POD group. Additionally, LPS-injected animal models and surgical models, both of which induce neuroinflammation with elevated cytokines and activated microglia, are widely recognized as classic animal models of delirium [32,33]. Therefore, we analyzed glial cell clusters from the human brain to investigate the relationship between the transcriptional state of glial cells and POD, with a particular focus on the neuroinflammatory state in the POD group. First, we analyzed microglial clusters, as microglia are the key cell type involved in neuroinflammation. A total of 12,859 nuclei were identified as microglia, characterized by the expression of representative markers CSF1R and P2RY12 **(Figure 3A, Figure 2C)**. Compared to the non-POD group, microglia in the POD group exhibited 332 significantly differentially expressed genes (DEGs), with 291 genes upregulated and 41 genes downregulated **(Figure 3B, Table S2)**. Gene Ontology (GO) biological process (BP) analysis identified 13 significantly enriched summary terms, many of which were immune-related **(Figure 3C)**. Pathway analysis further revealed that the “Neuroinflammatory Signaling Pathway” and “Interferon Alpha/Beta Signaling” were activated, while pathways known to suppress microglial immunological activation, such as “IL-10 Signaling” and “PPAR Alpha-related Signaling” [34,35] were inhibited **(Figure 3D)**. These findings present direct evidence showing that neuroinflammation was activated in the microglia of POD patients.

To determine which microglial subpopulations contributed to this transcriptional change, we performed a subcluster analysis. Recent studies have shown that disease-associated microglia (DAM) clusters emerge in both mice and humans with neuroinflammation-related neurodegenerative disorders, such as Alzheimer's disease [36–38]. We therefore focused on activated

microglia clusters resembling DAM to investigate microglial subpopulations in greater detail. Microglia were divided into nine subclusters **(Figure 3E)**, and the distribution of cells across subclusters was similar between the POD and non POD groups **(Figure S2A)**. To characterize these subclusters, we examined the expression of representative homeostatic and inflammation-related DAM markers[38]. Clusters 1 and 8 exhibited lower expressions of homeostatic genes and higher expressions of DAM-associated genes **(Figure 3F, Figure S2B)**. We also performed trajectory analysis to examine microglial transitions among subclusters. The greatest pseudotime changes relative to Cluster 0, which was considered the major homeostatic cluster, were observed in Clusters 1 and 8 **(Figure S2C)**. Since these findings suggest that these two DAM-like clusters represent more activated and pathological microglial subpopulations, these clusters were identified as inflammatory DAM (Inf-DAM) clusters. A total of 143 DEGs were enriched in Inf-DAM clusters, with 126 genes upregulated and 17 genes downregulated in the POD group **(Figure S2D, Table S3)**. Most of the 16 terms of GO BP analysis were again immune response-related terms **(Figure 3G)**. IPA pathway analysis further confirmed that neuroinflammation was strongly upregulated in Inf-DAM microglia in the POD group **(Figure 3H)**.

Recent studies have identified additional DAM subtypes, such as ribo-DAM (ribosome-related clusters) and lipo-DAM (lysosome and lipoprotein-related clusters) in human microglia[38]. Border-associated macrophage (BAM) shares the same origin (yolk sac) and similar profiles with microglia, but are distributed in the perivascular regions and choroid plexus, distinct from parenchymal microglia [39]. Therefore, we investigated whether the neuroinflammatory trend observed in the POD group extended to other microglial subclusters. Each subcluster was classified into five types (homeostatic, Inf-DAM, ribo-DAM, lipo-DAM, and BAM) based on the expression of representative markers **(Figure S2E, Figure 3F)**. In homeostatic microglia, enrichment analysis of 282 DEGs showed inflammatory trends such as the activation of "Neuroinflammation Signaling Pathway" and inhibition of IL-10 signaling and PPARα signaling", which suggested a potential pre-activation state in the POD group **(Figure S2F, G, Table S4)**. This may suggest that homeostatic microglia in the POD group were stated in the pre-activation state. In the BAM-like cluster, 120 genes were enriched **(Figure S2H, Table S5)**. In the pathway analysis, since only three pathways met our original criteria (q-value ≤ 0.01), we also considered terms with a q-value below 0.05, which were deemed statistically significant. These findings suggest that neuroinflammation was also promoted in the BAM-like cluster **(Figure S2I)**. In contrast, only five genes (*TMEM163, NAMPT, SAT1, MX1, GPCPD1*) were enriched in ribo-DAM, and no genes were found to be

enriched in lipo-DAM in the POD group. These findings indicate that POD-specific neuroinflammatory changes were widely occurring but unique in several subclusters to some extent.

Transcriptional profile of astrocyte in POD

Astrocytes are also thought to play a role in the pathogenesis of delirium, as suggested by previous studies in animal models [40,41] and humans [42,43]. In this study, we identified 16,080 nuclei as astrocytes based on the expression of representative markers GFAP and AQP4 **(Figure 4A, Figure 2C)**. Differential expression analysis revealed 734 DEGs in astrocytes from the POD group, including 536 upregulated and 198 downregulated genes **(Figure 4B, Table S6)**. GO BP analysis of astrocyte DEGs highlighted enrichment in synapse-related and morphogenesis-associated terms **(Figure 4C)**. Furthermore, IPA pathway analysis identified 52 enriched pathways, including 40 activated pathways, with synapse-related terms among the top-ranked **(Figure 4D)**. Unlike microglia, astrocytes did not show a predominant enrichment of neuroinflammation-related pathways

Reactive astrocytes, known as A1 astrocytes, are induced under neuroinflammatory conditions[44], Recent studies have also identified disease-associated astrocytes (DAAs), which emerge in pathological states[45]. Both of these subpopulations exhibit neurotoxic phenotypes in disease contexts[46]. Additionally, activation of astrocytes has been linked to delirium-like phenotypes in a POD mouse model[40]. Given these findings, we investigated how different astrocyte subpopulations contribute to POD-related transcriptomic changes.

Astrocytes were classified into five distinct clusters **(Figure 4E)**, with a comparable distribution of cells across subclusters in both the POD and non-POD groups **(Figure S3A)**. Based on the expression of key astrocyte activation markers (A1 and DAA markers)[46] and cluster distribution in UMAP, we characterized these subclusters as homeostatic astrocytes (clusters 1 and 2) and activated astrocytes (clusters 0 and 4) **(Figure 4F)**. In homeostatic astrocytes, we identified 1,117 DEGs **(Figure S3B, Table S7)**, which were subjected to enrichment analysis. GO BP and pathway analyses revealed significant enrichment in synapse- and neurotransmitter-related terms **(Figure S3C, Figure 4G)**. In contrast, the 734 DEGs identified in activated astrocytes **(Figure S3D, Table S8)** displayed a distinct profile, with migration-related terms being enriched and RHO GTPase signaling pathways showing characteristic upregulation **(Figure 4H, Figure S3E)**.

Transcriptional profile of OPC and Oligodendrocyte in POD

Although the role of OPCs and oligodendrocytes in POD remains less clear compared to microglia and astrocytes, they may contribute to delirium pathogenesis through white matter dysfunction[31]. Our dataset included 8,305 nuclei classified as OPCs, characterized by the expression of the representative marker PDGFRA **(Figure S4A, Figure 2C)**. Analysis of 185 DEGs **(Figure S4B, Table S9)** revealed enrichment in several GO BP and pathway terms, including synaptic transmission-related processes **(Figure S4C, D)**. A total of 39,585 nuclei were identified as oligodendrocytes, specifically expressing MOG and MOBP **(Figure S4E, Figure 2C)**. Although 92 DEGs were detected in the POD group **(Figure S4F, Table S10)**, no significant GO or pathway terms were enriched. This suggests that, compared to other cell types, oligodendrocytes exhibit minimal transcriptional changes associated with POD.

Downstream analysis of glial cells

According to the results of the DEG and enrichment analyses, microglia and astrocytes exhibited significant transcriptomic changes in the POD group. To assess the relationship between these changes and POD pathogenesis, we conducted disease and function enrichment analysis as a downstream analysis using the DEG lists from each cell cluster. To investigate the pathological similarities between POD and other brain-related disorders, we focused on neurological disease-associated terms that were significantly activated in the POD group (q-value < 0.01 and z-score > 1). In whole microglia, all eight enriched terms were associated with inflammation or encephalitis **(Figure 5A)**. Similarly, encephalitis-related terms were also enriched in homeostatic microglia and inflammatory DAM **(Figure 5B, C)**. Additionally, the term "cognitive impairment" was significantly enriched in homeostatic microglia, while a demyelination-related term was identified in inflammatory DAM.

Enriched terms in the whole astrocyte population were primarily related to glioma and inflammation **(Figure 5D)**, whereas homeostatic astrocytes exhibited a distinct pattern **(Figure 5E)**. The only shared term between these two clusters was "Cognitive impairment." Notably, no neurological disease-related terms were identified as upregulated in activated astrocytes.

Because delirium and dementia are often considered closely related[47], and some glial subclusters enriched "Cognitive impairment" as expected, we further investigate the relationship between glial cells in POD and dementia, we assessed the statistical significance of five dementia-associated terms across each cell cluster **(Figure S5)**. In microglia clusters, two to three terms were significantly enriched in each cluster, suggesting that microglia in the POD group broadly exhibit

transcriptional changes associated with dementia. In contrast, four to five dementia-related terms were significantly enriched in whole astrocytes and activated astrocytes, whereas none were detected in homeostatic astrocytes. This finding indicates that activated astrocytes exhibit a strong and specific transcriptional overlap with dementia pathology.

Discussion

This study is the first to integrate DNA methylation profiling and snRNAseq in brain tissues from POD patients, providing direct molecular evidence of glial involvement in POD pathogenesis. Unlike previous studies that relied on peripheral samples or postmortem tissues, our analysis offers real-time insights from living brain tissues, allowing us to capture early molecular changes prior to delirium onset.

Our DNA methylation analysis revealed noticeable alterations in the POD group even very early on shortly after brain tissue resection and before the onset of delirium. Notably, enhanced demethylation was observed in highly methylated regions of immune-related genes, suggesting that immune response enhancement leading to POD may be regulated at the epigenetic level. Furthermore, our previous study from the same cohort has identified immune-related epigenetic changes in blood samples immediately after the brain resection surgery[9], which were also observed in multiple other cohorts with delirium of different etiologies [30,48]. This suggests that similar DNA methylation alterations found in the brain may be similarly detectable in the blood, raising the possibility of utilizing blood DNA methylation patterns as predictive biomarkers for delirium onset.

Our snRNAseq analysis revealed POD-specific transcriptional changes, particularly in microglia and astrocytes, whereas no significant pathway enrichment was observed in oligodendrocytes. This suggests that cell-type specificity exists in the early stages of POD pathogenesis. In microglia, we observed a strong and widespread activation of neuroinflammatory pathways. Previous studies have suggested the involvement of neuroinflammation in POD, reporting upregulated inflammatory markers such as pro-inflammatory cytokines in cerebrospinal fluid[49,50] and postmortem brain samples[42]. While these studies indirectly linked neuroinflammation to POD, our findings provide the first direct evidence of enhanced neuroinflammatory responses in microglia during POD pathogenesis. Additionally, our enrichment analysis revealed inhibition of PPARα signaling in microglia, particularly in homeostatic microglia. PPARα signaling is known to have suppressive effects on microglial activation[51,52]. This suggests that PPARα suppression may increase microglial susceptibility to a pro-inflammatory state, thereby promoting POD

pathogenesis. These findings also raise the possibility that PPARα agonists could have a preventive effect on POD.

Regarding astrocytes, multiple signaling pathways were enriched in the POD group. Astrocytes play diverse roles, including regulating synaptic activity and neurotransmission, maintaining the blood-brain barrier (BBB), mediating neuroinflammation, and energy metabolism [31,53]. In homeostatic astrocytes, synapse-related pathways were upregulated, which may contribute to excitatory-inhibitory imbalance, a fundamental mechanism implicated in delirium[54]. Conversely, activated astrocytes exhibited RHO GTPase upregulation and enrichment of migration-related pathways. In general, RHO GTPase negatively regulates astrocyte migration[55], whereas inflammatory stimulation is known to inhibit RHO GTPase and promote astrogliosis[56]. However, our findings showed heightened RHO GTPase activity in POD astrocytes, suggesting that RHO GTPase activity and the altered migration may suppress POD pathogenesis.

Downstream analysis revealed that POD-associated microglia and astrocytes share common transcriptional trends with several diseases, suggesting that therapeutic strategies used for related conditions may be applicable to POD treatment. The transcriptional profile of microglia in the POD group closely resembled that observed in encephalitis. While microglia are known to play both protective and detrimental roles in encephalitis, they are critical mediators of the disease process[57]. This similarity suggests that microglia may exhibit comparable behaviors in encephalitis and POD pathogenesis. Astrocytes were also implicated in inflammatory pathology, although their subclusters did not show a clear trend. Furthermore, the downstream analysis highlighted a potential link between dementia and POD. The term “cognitive impairment” was significantly enriched in both microglia and astrocyte clusters, and multiple dementia-related terms were also significantly enriched. These findings support the hypothesis of a shared pathological mechanism between dementia and POD.

This study has several limitations. First, the small sample size (18 subjects, including 9 POD patients) limits statistical power. However, analyzing brain tissue from living patients offers a unique opportunity to directly study POD pathology. To the best of our knowledge, this is the first multi-omics analysis of POD patient brain samples, marking an important step toward understanding its molecular mechanisms. Future studies with larger cohorts will be needed to validate these findings. Second, due to sample size limitations, we did not examine sex- and age-dependent differences. While age is a well-known risk factor for delirium, the influence of sex remains controversial [58,59]. Larger studies incorporating these variables will be essential for a

comprehensive understanding of POD pathogenesis. Third, no single CpG site reached genome-wide significance, likely due to the small sample size. Additionally, the challenge of detecting significant differences may stem from cell-type mixture in bulk methylation data, emphasizing the need for cell-type-specific epigenomic analyses. Nonetheless, potential CpG clusters in our analysis displayed unique characteristics related to POD, warranting further investigation. Lastly, our snRNAseq analysis focused on glial cells, leaving neurons largely unexamined. Given the nature of the resected brain tissue from epilepsy focal resection surgery, sample variability across brain regions resulted in diverse neuronal characteristics, making analysis challenging. However, since neural activity is correlated with POD[60], targeted neuronal analysis will be crucial in future studies.

Despite these limitations, our study provides new insights into the molecular underpinnings of POD pathogenesis, highlighting the direct role of glial cells in disease development. By integrating DNA methylation and snRNAseq analysis, we uncovered direct evidence of epigenetic and transcriptomic mechanisms associated with neuroinflammation and more in POD. These findings suggest novel therapeutic strategies, particularly targeting microglia and astrocytes, to mitigate POD risk and improve patient outcomes.

Data availability

DNA methylation data and snRNAseq data have been deposited in the Gene Expression Omnibus database (GSE290719, GSE291019). Other processed data generated in the present study are available from the corresponding author, G.S., upon reasonable request.

Acknowledgments

The authors appreciate the patients who participated in this study. This work was supported by research grants from the National Institute of Mental Health, United States (R01 MH119165, AG084710).

References

1. Thein, A., Pereira, M. Z., Nitchingham, J. V. & Caplan, A. A call to action for delirium research: meta-analysis and regression of delirium associated mortality. *BMC Geriatr* **20**, 1–12 (2020).

2. Leslie, D. L. & Inouye, S. K. The importance of delirium: economic and societal costs. *J. Am. Geriatr. Soc.* **59 Suppl 2**, S241-3 (2011).
3. Mohanty, S. *et al.* Major surgery and long term cognitive outcomes: The effect of postoperative delirium on dementia in the year following discharge. *J. Surg. Res.* **270**, 327–334 (2022).
4. Nishizawa, Y. *et al.* Epigenetic signals associated with delirium replicated across four independent cohorts. *Transl. Psychiatry* **14**, 275 (2024).
5. Wahba, N. E. *et al.* Genome-wide DNA methylation analysis of post-operative delirium with brain, blood, saliva, and buccal samples from neurosurgery patients. *J. Psychiatr. Res.* **156**, 245–251 (2022).
6. Cuevas-Diaz Duran, R., González-Orozco, J. C., Velasco, I. & Wu, J. Q. Single-cell and single-nuclei RNA sequencing as powerful tools to decipher cellular heterogeneity and dysregulation in neurodegenerative diseases. *Front. Cell Dev. Biol.* **10**, 884748 (2022).
7. Walter, T. J., Suter, R. K. & Ayad, N. G. An overview of human single-cell RNA sequencing studies in neurobiological disease. *Neurobiol. Dis.* **184**, 106201 (2023).
8. Shi, Y. & Xu, P. Unveiling the immune landscape of delirium through single-cell RNA sequencing and machine learning: Towards precision diagnosis and therapy. *Psychogeriatrics* **25**, e13233 (2025).
9. Yamanashi, T. *et al.* The genome-wide DNA methylation profiles among neurosurgery patients with and without post-operative delirium. *Psychiatry Clin. Neurosci.* **77**, 48–55 (2023).
10. Inouye, S. K. *et al.* A chart-based method for identification of delirium: validation compared with interviewer ratings using the confusion assessment method. *J. Am. Geriatr. Soc.* **53**, 312–318 (2005).

11. Zhou, B. *et al.* Detection and analysis of complex structural variation in human genomes across populations and in brains of donors with psychiatric disorders. *Cell* **187**, 6687-6706.e25 (2024).
12. Core, R. T. R: A language and environment for statistical computing. *(No Title)* (2019).
13. Morris, T. J. *et al.* ChAMP: 450k chip analysis methylation pipeline. *Bioinformatics* **30**, 428–430 (2014).
14. Tian, Y. *et al.* ChAMP: updated methylation analysis pipeline for Illumina BeadChips. *Bioinformatics* **33**, 3982–3984 (2017).
15. Aryee, M. J. *et al.* Minfi: a flexible and comprehensive Bioconductor package for the analysis of Infinium DNA methylation microarrays. *Bioinformatics* **30**, 1363–1369 (2014).
16. Fortin, J.-P., Triche, T. J., Jr & Hansen, K. D. Preprocessing, normalization and integration of the Illumina HumanMethylationEPIC array with minfi. *Bioinformatics* **33**, 558–560 (2017).
17. Teschendorff, A. E. *et al.* A beta-mixture quantile normalization method for correcting probe design bias in Illumina Infinium 450 k DNA methylation data. *Bioinformatics* **29**, 189–196 (2013).
18. Assenov, Y. *et al.* Comprehensive analysis of DNA methylation data with RnBeads. *Nat. Methods* **11**, 1138–1140 (2014).
19. Ritchie, M. E. *et al.* limma powers differential expression analyses for RNA-sequencing and microarray studies. *Nucleic Acids Res.* **43**, e47 (2015).
20. Hao, Y. *et al.* Dictionary learning for integrative, multimodal and scalable single-cell analysis. *Nat. Biotechnol.* **42**, 293–304 (2024).
21. Thrupp, N. *et al.* Single-nucleus RNA-seq is not suitable for detection of microglial activation genes in humans. *Cell Rep.* **32**, 108189 (2020).
22. Del-Aguila, J. L. *et al.* A single-nuclei RNA sequencing study of Mendelian and sporadic AD

in the human brain. *Alzheimers. Res. Ther.* **11**, 71 (2019).

23. Ayhan, F. *et al.* Resolving cellular and molecular diversity along the hippocampal anterior-to-posterior axis in humans. *Neuron* **109**, 2091-2105.e6 (2021).
24. Trapnell, C. *et al.* The dynamics and regulators of cell fate decisions are revealed by pseudotemporal ordering of single cells. *Nat. Biotechnol.* **32**, 381–386 (2014).
25. Qiu, X. *et al.* Reversed graph embedding resolves complex single-cell trajectories. *Nat. Methods* **14**, 979–982 (2017).
26. Cao, J. *et al.* The single-cell transcriptional landscape of mammalian organogenesis. *Nature* **566**, 496–502 (2019).
27. McInnes, L., Healy, J. & Melville, J. UMAP: Uniform Manifold Approximation and Projection for Dimension Reduction. *arXiv [stat.ML]* (2018).
28. Zhou, Y. *et al.* Metascape provides a biologist-oriented resource for the analysis of systems-level datasets. *Nat. Commun.* **10**, 1523 (2019).
29. Phipson, B., Maksimovic, J. & Oshlack, A. missMethyl: an R package for analyzing data from Illumina's HumanMethylation450 platform. *Bioinformatics* **32**, 286–288 (2016).
30. Nishizawa, Y. *et al.* The Genome-wide DNA methylation changes in gastrointestinal surgery patients with and without postoperative delirium: Evidence of immune process in its pathophysiology. *J. Psychiatr. Res.* **177**, 249–255 (2024).
31. Heffernan, Á. B. *et al.* Role of glia in delirium: proposed mechanisms and translational implications. *Mol. Psychiatry* (2024) doi:10.1038/s41380-024-02801-4.
32. Vasunilashorn, S. M. *et al.* Preclinical and translational models for delirium: Recommendations for future research from the NIDUS delirium network. *Alzheimers. Dement.* **19**, 2150–2174 (2023).
33. Nishiguchi, T. *et al.* Lipopolysaccharide-induced delirium-like behavior and microglial

activation in mice correlate with bispectral electroencephalography. *J. Gerontol. A Biol. Sci. Med. Sci.* **79**, (2024).

34. Choi, M.-J. *et al.* Anti-inflammatory mechanism of galangin in lipopolysaccharide-stimulated microglia: Critical role of PPAR-γ signaling pathway. *Biochem. Pharmacol.* **144**, 120–131 (2017).
35. Shemer, A. *et al.* Interleukin-10 prevents pathological microglia hyperactivation following peripheral endotoxin challenge. *Immunity* **53**, 1033-1049.e7 (2020).
36. Keren-Shaul, H. *et al.* A unique microglia type associated with restricting development of Alzheimer's disease. *Cell* **169**, 1276-1290.e17 (2017).
37. Deczkowska, A. *et al.* Disease-associated microglia: A universal immune sensor of neurodegeneration. *Cell* **173**, 1073–1081 (2018).
38. Martins-Ferreira, R. *et al.* The Human Microglia Atlas (HuMicA) unravels changes in disease-associated microglia subsets across neurodegenerative conditions. *Nat. Commun.* **16**, 739 (2025).
39. Utz, S. G. *et al.* Early fate defines microglia and non-parenchymal brain macrophage development. *Cell* **181**, 557-573.e18 (2020).
40. Liu, W. *et al.* Increased A1 astrocyte activation-driven hippocampal neural network abnormality mediates delirium-like behavior in aged mice undergoing cardiac surgery. *Aging Cell* **23**, e14074 (2024).
41. Jin, W.-J. *et al.* Minocycline improves postoperative cognitive impairment in aged mice by inhibiting astrocytic activation. *Neuroreport* **25**, 1–6 (2014).
42. Munster, B. *et al.* Neuroinflammation in delirium: a postmortem case-control study. *Rejuvenation Res.* **14**, 615–622 (2011).
43. Bassi, T., Rohrs, E., Nicholas, M. & Reynolds, S. Meta-analysis of serological biomarkers at

hospital admission for the likelihood of developing delirium during hospitalization. *Front. Neurol.* **14**, 1179243 (2023).

44. Liddelow, S. A. *et al.* Neurotoxic reactive astrocytes are induced by activated microglia. *Nature* **541**, 481–487 (2017).
45. Habib, N. *et al.* Disease-associated astrocytes in Alzheimer's disease and aging. *Nat. Neurosci.* **23**, 701–706 (2020).
46. Yu, W. *et al.* Disease-associated neurotoxic astrocyte markers in Alzheimer disease based on integrative single-nucleus RNA sequencing. *Cell. Mol. Neurobiol.* **44**, 20 (2024).
47. Fong, T. G. & Inouye, S. K. The inter-relationship between delirium and dementia: the importance of delirium prevention. *Nat. Rev. Neurol.* **18**, 579–596 (2022).
48. Saito, T. *et al.* Epigenetics of neuroinflammation: Immune response, inflammatory response and cholinergic synaptic involvement evidenced by genome-wide DNA methylation analysis of delirious inpatients. *J. Psychiatr. Res.* **129**, 61–65 (2020).
49. Cape, E. *et al.* Cerebrospinal fluid markers of neuroinflammation in delirium: a role for interleukin-1β in delirium after hip fracture. *J. Psychosom. Res.* **77**, 219–225 (2014).
50. Hirsch, J. *et al.* Perioperative cerebrospinal fluid and plasma inflammatory markers after orthopedic surgery. *J. Neuroinflammation* **13**, (2016).
51. Ogawa, K. *et al.* Pemafibrate, a selective PPARα modulator, and fenofibrate suppress microglial activation through distinct PPARα and SIRT1-dependent pathways. *Biochem. Biophys. Res. Commun.* **524**, 385–391 (2020).
52. Yuan, T. *et al.* The protective role of microglial PPARα in diabetic retinal neurodegeneration and neurovascular dysfunction. *Cells* **11**, 3869 (2022).
53. Verkhratsky, A. & Nedergaard, M. Physiology of astroglia. *Physiol. Rev.* **98**, 239–389 (2018).
54. Wilson, J. E. *et al.* Delirium. *Nat. Rev. Dis. Primers* **6**, 90 (2020).

55. Höltje, M. *et al.* Role of Rho GTPase in astrocyte morphology and migratory response during in vitro wound healing. *J. Neurochem.* **95**, 1237–1248 (2005).

56. John, G. R. *et al.* Interleukin-1beta induces a reactive astroglial phenotype via deactivation of the Rho GTPase-Rock axis. *J. Neurosci.* **24**, 2837–2845 (2004).

57. Waltl, I. & Kalinke, U. Beneficial and detrimental functions of microglia during viral encephalitis. *Trends Neurosci.* **45**, 158–170 (2022).

58. Wang, H. *et al.* Gender differences and postoperative delirium in adult patients undergoing cardiac valve surgery. *Front. Cardiovasc. Med.* **8**, 751421 (2021).

59. Wiredu, K. *et al.* Sex differences in the incidence of postoperative delirium after cardiac surgery: A pooled analyses of clinical trials. *Anesthesiology* **139**, 540–542 (2023).

60. Tanabe, S. *et al.* Cohort study into the neural correlates of postoperative delirium: the role of connectivity and slow-wave activity. *Br. J. Anaesth.* **125**, 55–66 (2020).

Table 1. Subject characteristics

Classification	All Subjects	POD	non-POD	*P*	
N	18	9	9		Statistical test
Mean age (years)	36.4	39.9	30.8	0.33	t = 1.007
SD	14.1	16.0	11.7		
Sex (Female) (n)	7	4	3	0.63	$\chi^2 = 0.2338$
%	38.9	44.4	33.3		
BMI (kg/m^2)	29.0	28.3	29.6	0.75	t = -0.3251
SD	8.5	7.7	9.6		
Mean anesthesia time (min)	542.6	545.9	539.2	0.84	t = 0.2126 (unequal variance)
SD	64.6	84.5	41.4		
Mean procedure time (min)	352.2	360.0	344.4	0.68	t = 0.4192 (unequal variance)
SD	76.8	100.0	49.0		
Mean blood loss (mL)	182.5	175.0	209.4	0.47	t = -0.7436
SD	151.7	171.7	133.3		
History of alcohol use (n)	6	3	3	1.00	Fisher's exact test OR= 1.000, 95% CI [0.0919,10.88]
%	33.3	33.3	33.3		
History of tobacco use (n)	8	5	3	0.64	Fisher's exact test
%	44.4	55.5	33.3		OR= 2.372, 95% CI [0.2652, 25.53]

BMI, Body mass index; POD, post-operative delirium; SD, Standard deviation; OR, Odds Ratio; CI, Confidence Interval

Table 2. Top 20 terms of GO BP and KEGG pathway analysis with all differentially methylated CpGs (p <0.05)

GO					
GO Term	Description	N	DE	P.DE	FDR
GO:0007162	negative regulation of cell adhesion	311	64	1.30E-05	0.297
GO:0048704	embryonic skeletal system morphogenesis	95	27	1.22E-04	1
GO:0030217	T cell differentiation	300	57	1.81E-04	1
GO:0022408	negative regulation of cell-cell adhesion	204	38	8.61E-04	1
GO:1903706	regulation of hemopoiesis	411	68	1.25E-03	1
GO:0045580	regulation of T cell differentiation	180	36	1.42E-03	1
GO:0050865	regulation of cell activation	648	97	1.55E-03	1
GO:0045619	regulation of lymphocyte differentiation	211	40	1.71E-03	1
GO:0042110	T cell activation	545	84	1.77E-03	1
GO:0071674	mononuclear cell migration	199	34	1.78E-03	1
GO:0050868	negative regulation of T cell activation	130	24	2.01E-03	1
GO:0050856	regulation of T cell receptor signaling pathway	44	12	2.10E-03	1
GO:0048706	embryonic skeletal system development	128	30	2.10E-03	1
GO:0007264	small GTPase mediated signal transduction	480	91	2.18E-03	1
GO:0060284	regulation of cell development	827	132	2.38E-03	1
GO:1903774	positive regulation of viral budding via host ESCRT complex	3	3	2.44E-03	1
GO:0032874	positive regulation of stress-activated MAPK cascade	129	28	2.56E-03	1
GO:0045606	positive regulation of epidermal cell differentiation	28	9	2.59E-03	1
GO:1902105	regulation of leukocyte differentiation	318	54	2.96E-03	1
GO:0045321	leukocyte activation	933	130	3.29E-03	1
KEGG Pathway					

KEGG Term	Description	N	DE	P.DE	FDR
hsa04724	Glutamatergic synapse	116	28	1.15E-02	0.729
hsa04015	Rap1 signaling pathway	210	43	1.19E-02	0.729
hsa04911	Insulin secretion	86	21	1.22E-02	0.729
hsa04940	Type I diabetes mellitus	42	11	1.32E-02	0.729
hsa04270	Vascular smooth muscle contraction	134	27	1.45E-02	0.729
hsa04921	Oxytocin signaling pathway	154	33	1.52E-02	0.729
hsa04935	Growth hormone synthesis, secretion and action	121	27	1.59E-02	0.729
hsa04062	Chemokine signaling pathway	192	33	1.96E-02	0.729
hsa05031	Amphetamine addiction	69	16	2.29E-02	0.729
hsa04261	Adrenergic signaling in cardiomyocytes	152	31	2.44E-02	0.729
hsa05412	Arrhythmogenic right ventricular cardiomyopathy	86	21	2.62E-02	0.729
hsa05100	Bacterial invasion of epithelial cells	77	18	2.77E-02	0.729
hsa04927	Cortisol synthesis and secretion	65	16	3.00E-02	0.729
hsa04962	Vasopressin-regulated water reabsorption	44	10	3.04E-02	0.729
hsa05414	Dilated cardiomyopathy	104	23	3.15E-02	0.729
hsa04914	Progesterone-mediated oocyte maturation	98	19	3.22E-02	0.729
hsa04530	Tight junction	170	30	3.90E-02	0.760
hsa05163	Human cytomegalovirus infection	225	38	4.36E-02	0.760
hsa04371	Apelin signaling pathway	139	26	4.82E-02	0.760
hsa03450	Non-homologous end-joining	13	4	4.86E-02	0.760

Note: Immune/Inflammation-related terms are underlined

KEGG, Kyoto Encyclopedia of Genes and Genomes

Table 3. Top terms of GO BP and KEGG analysis with differentially methylated CpGs (age-associated CpGs)

GO					
GO Term	Description	N	DE	P.DE	FDR
GO:0002876	positive regulation of chronic inflammatory response to antigenic stimulus	2	2	1.14E-05	0.194
GO:0002439	chronic inflammatory response to antigenic stimulus	3	2	2.55E-05	0.194
GO:0002874	regulation of chronic inflammatory response to antigenic stimulus	3	2	2.55E-05	0.194
GO:0002678	positive regulation of chronic inflammatory response	4	2	6.52E-05	0.373
GO:0032741	positive regulation of interleukin-18 production	7	2	1.86E-04	0.853
GO:1902565	positive regulation of neutrophil activation	6	2	3.04E-04	1
GO:0002925	positive regulation of humoral immune response mediated by circulating immunoglobulin	7	2	3.93E-04	1
GO:2000343	positive regulation of chemokine (C-X-C motif) ligand 2 production	9	2	6.60E-04	1
GO:0032621	interleukin-18 production	13	2	6.76E-04	1
GO:0032661	regulation of interleukin-18 production	13	2	6.76E-04	1
GO:1903223	positive regulation of oxidative stress-induced neuron death	8	2	6.87E-04	1
GO:0002676	regulation of chronic inflammatory response	10	2	7.60E-04	1
GO:0032755	positive regulation of interleukin-6 production	99	4	9.00E-04	1
GO:0071803	positive regulation of podosome assembly	10	2	1.10E-03	1
GO:0070305	response to cGMP	9	2	1.71E-03	1
GO:0060251	regulation of glial cell proliferation	39	3	1.84E-03	1
GO:0002863	positive regulation of inflammatory response to antigenic stimulus	13	2	1.95E-03	1
GO:0033477	S-methylmethionine metabolic process	1	1	1.97E-03	1
GO:1902563	regulation of neutrophil activation	15	2	2.03E-03	1
GO:0042756	drinking behavior	12	2	2.07E-03	1
KEGG Pathway					

KEGG Term	Description	N	DE	P.DE	FDR
hsa04940	Type I diabetes mellitus	42	3	2.13E-03	0.617
hsa04625	C-type lectin receptor signaling pathway	104	4	3.41E-03	0.617
hsa04144	Endocytosis	249	6	5.60E-03	0.676
hsa05143	African trypanosomiasis	36	2	1.15E-02	0.799
hsa05152	Tuberculosis	178	4	1.19E-02	0.799
hsa05235	PD-L1 expression and PD-1 checkpoint pathway in cancer	89	3	1.75E-02	0.799
hsa04064	NF-kappa B signaling pathway	104	3	1.80E-02	0.799
hsa05142	Chagas disease	102	3	1.89E-02	0.799
hsa05144	Malaria	50	2	1.99E-02	0.799
hsa04650	Natural killer cell mediated cytotoxicity	125	3	2.64E-02	0.871
hsa04061	Viral protein interaction with cytokine and cytokine receptor	99	2	2.65E-02	0.871
hsa05321	Inflammatory bowel disease	64	2	4.28E-02	1
hsa04660	T cell receptor signaling pathway	118	3	4.61E-02	1

Note: Immune/Inflammation-related terms are underlined

Table 4. Top 20 terms of GO BP and KEGG analysis with differentially methylated CpGs (high-methylated, down)

GO Term	Description	N	DE	P.DE	FDR
GO					
GO:0002250	adaptive immune response	450	28	2.60E-06	0.059
GO:0032874	positive regulation of stress-activated MAPK cascade	129	15	9.11E-06	0.074
GO:0050856	regulation of T cell receptor signaling pathway	44	8	1.13E-05	0.074
GO:0070304	positive regulation of stress-activated protein kinase signaling cascade	131	15	1.29E-05	0.074
GO:0050854	regulation of antigen receptor-mediated signaling pathway	65	9	4.33E-05	0.167
GO:0046330	positive regulation of JNK cascade	95	12	5.86E-05	0.167
GO:0042110	T cell activation	545	31	6.55E-05	0.167
GO:0046649	lymphocyte activation	768	39	7.85E-05	0.180
GO:0045321	leukocyte activation	933	44	9.48E-05	0.185
GO:0022408	negative regulation of cell-cell adhesion	204	16	9.71E-05	0.185
GO:1903038	negative regulation of leukocyte cell-cell adhesion	149	12	1.44E-04	0.236
GO:0002252	immune effector process	628	30	1.75E-04	0.264
GO:0050868	negative regulation of T cell activation	130	11	1.85E-04	0.264
GO:0032872	regulation of stress-activated MAPK cascade	192	16	2.75E-04	0.336
GO:0002876	positive regulation of chronic inflammatory response to antigenic stimulus	2	2	2.77E-04	0.336
GO:0098609	cell-cell adhesion	945	48	2.79E-04	0.336
GO:1901222	regulation of NIK/NF-kappaB signaling	110	9	3.28E-04	0.368
GO:0050860	negative regulation of T cell receptor signaling pathway	25	5	3.37E-04	0.368
GO:0070302	regulation of stress-activated protein kinase signaling cascade	195	16	3.56E-04	0.371
GO:0006955	immune response	1631	58	3.87E-04	0.376
KEGG Pathway					

KEGG Term	Description	N	DE	P.DE	FDR
hsa04064	NF-kappa B signaling pathway	104	11	1.07E-04	0.039
hsa04659	Th17 cell differentiation	107	9	6.61E-03	0.542
hsa04976	Bile secretion	89	7	8.71E-03	0.542
hsa04940	Type I diabetes mellitus	42	5	8.80E-03	0.542
hsa04060	Cytokine-cytokine receptor interaction	293	11	8.87E-03	0.542
hsa04514	Cell adhesion molecules	153	11	9.89E-03	0.542
hsa04061	Viral protein interaction with cytokine and cytokine receptor	99	5	1.05E-02	0.542
hsa04270	Vascular smooth muscle contraction	134	10	1.20E-02	0.542
hsa04668	TNF signaling pathway	118	8	1.68E-02	0.637
hsa04650	Natural killer cell mediated cytotoxicity	125	8	1.76E-02	0.637
hsa05321	Inflammatory bowel disease	64	5	2.43E-02	0.735
hsa05310	Asthma	29	3	2.53E-02	0.735
hsa04914	Progesterone-mediated oocyte maturation	98	7	2.83E-02	0.735
hsa04062	Chemokine signaling pathway	192	11	2.84E-02	0.735
hsa05152	Tuberculosis	178	9	3.48E-02	0.829
hsa04625	C-type lectin receptor signaling pathway	104	7	3.66E-02	0.829
hsa04080	Neuroactive ligand-receptor interaction	366	13	4.01E-02	0.855
hsa04622	RIG-I-like receptor signaling pathway	72	4	4.96E-02	0.990

Note: Immune/Inflammation-related terms are underlined.

Table 5. Top 20 terms of GO BP and KEGG analysis with differentially methylated CpGs (low-methylated, up)

GO					
GO Term	Description	N	DE	P.DE	FDR
GO:0048704	embryonic skeletal system morphogenesis	95	21	2.30E-07	0.005
GO:0048706	embryonic skeletal system development	128	24	9.39E-07	0.011
GO:0048705	skeletal system morphogenesis	226	30	5.34E-05	0.262
GO:0009952	anterior/posterior pattern specification	209	26	8.94E-05	0.336
GO:0048857	neural nucleus development	64	12	1.17E-04	0.336
GO:0007399	nervous system development	2492	186	2.57E-04	0.478
GO:0045606	positive regulation of epidermal cell differentiation	28	7	3.24E-04	0.484
GO:0010159	specification of animal organ position	3	3	3.35E-04	0.484
GO:0003002	regionalization	421	41	3.59E-04	0.484
GO:0007389	pattern specification process	466	45	3.64E-04	0.484
GO:0048523	negative regulation of cellular process	4882	291	6.03E-04	0.640
GO:0032026	response to magnesium ion	19	6	6.90E-04	0.640
GO:0048598	embryonic morphogenesis	612	56	7.87E-04	0.640
GO:0031327	negative regulation of cellular biosynthetic process	1656	110	8.11E-04	0.640
GO:0000122	negative regulation of transcription by RNA polymerase II	949	73	8.70E-04	0.641
GO:0061140	lung secretory cell differentiation	11	4	8.96E-04	0.641
GO:2000480	negative regulation of cAMP-dependent protein kinase activity	13	5	9.36E-04	0.641
GO:0045684	positive regulation of epidermis development	33	7	9.53E-04	0.641
GO:0072125	negative regulation of glomerular mesangial cell proliferation	4	3	1.03E-03	0.641
GO:0009890	negative regulation of biosynthetic process	1686	111	1.03E-03	0.641
KEGG Pathway					

KEGG Term	Description	N	DE	P.DE	FDR
hsa04919	Thyroid hormone signaling pathway	121	19	4.46E-04	0.162
hsa04015	Rap1 signaling pathway	210	24	5.28E-03	0.538
hsa04935	Growth hormone synthesis, secretion and action	121	16	5.79E-03	0.538
hsa04970	Salivary secretion	93	11	9.72E-03	0.538
hsa04911	Insulin secretion	86	12	1.06E-02	0.538
hsa04927	Cortisol synthesis and secretion	65	10	1.14E-02	0.538
hsa04211	Longevity regulating pathway	89	12	1.23E-02	0.538
hsa04918	Thyroid hormone synthesis	75	10	1.38E-02	0.538
hsa04261	Adrenergic signaling in cardiomyocytes	152	17	1.72E-02	0.538
hsa04961	Endocrine and other factor-regulated calcium reabsorption	53	8	2.24E-02	0.538
hsa05221	Acute myeloid leukemia	67	9	2.36E-02	0.538
hsa03450	Non-homologous end-joining	13	3	2.41E-02	0.538
hsa04072	Phospholipase D signaling pathway	147	17	2.42E-02	0.538
hsa04928	Parathyroid hormone synthesis, secretion and action	115	14	2.45E-02	0.538
hsa04022	cGMP-PKG signaling pathway	165	17	2.51E-02	0.538
hsa04921	Oxytocin signaling pathway	154	17	2.53E-02	0.538
hsa04962	Vasopressin-regulated water reabsorption	44	6	2.66E-02	0.538
hsa04915	Estrogen signaling pathway	137	14	2.68E-02	0.538
hsa05205	Proteoglycans in cancer	202	20	2.85E-02	0.544
hsa04371	Apelin signaling pathway	139	14	3.75E-02	0.600

Note: Immune/Inflammation-related terms are underlined

Figure 1.

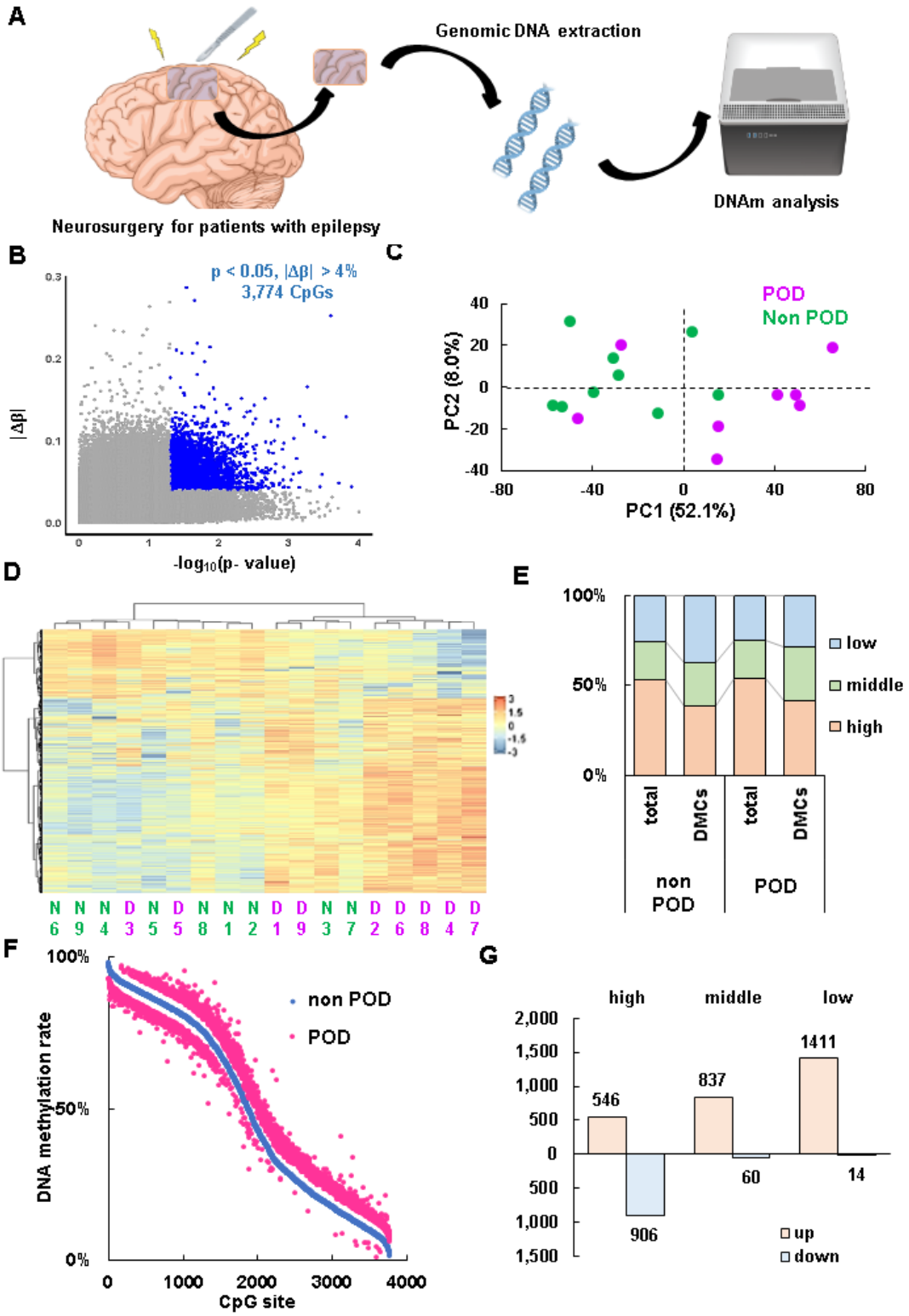

Figure 1. DNA methylation changes between non POD and POD group

A Research scheme for DNA methylation analysis using resected brain tissue

B Volcano plot displaying 3,774 differently methylated CpGs (DMCs) with a p-value < 0.05 and delta beta value > 4%

C Principal component analysis of DMCs using Z-score of the beta values

D Hierarchical clustering heatmap representing DNA methylation of DMCs. Z-score of the beta values is shown. N1-9 represent non-POD subjects and D1-9 represent POD subjects.

E Distribution of methylation rate; high: 70%>, low: 30%<. Middle: 30-70%

F The plot shows the methylation rates (β-values) of CpG sites in the POD group (blue) and non-POD group (magenta). The x-axis represents individual CpG sites, while the y-axis indicates the methylation rate.

G DNA methylation rate of each DMC

Figure 2

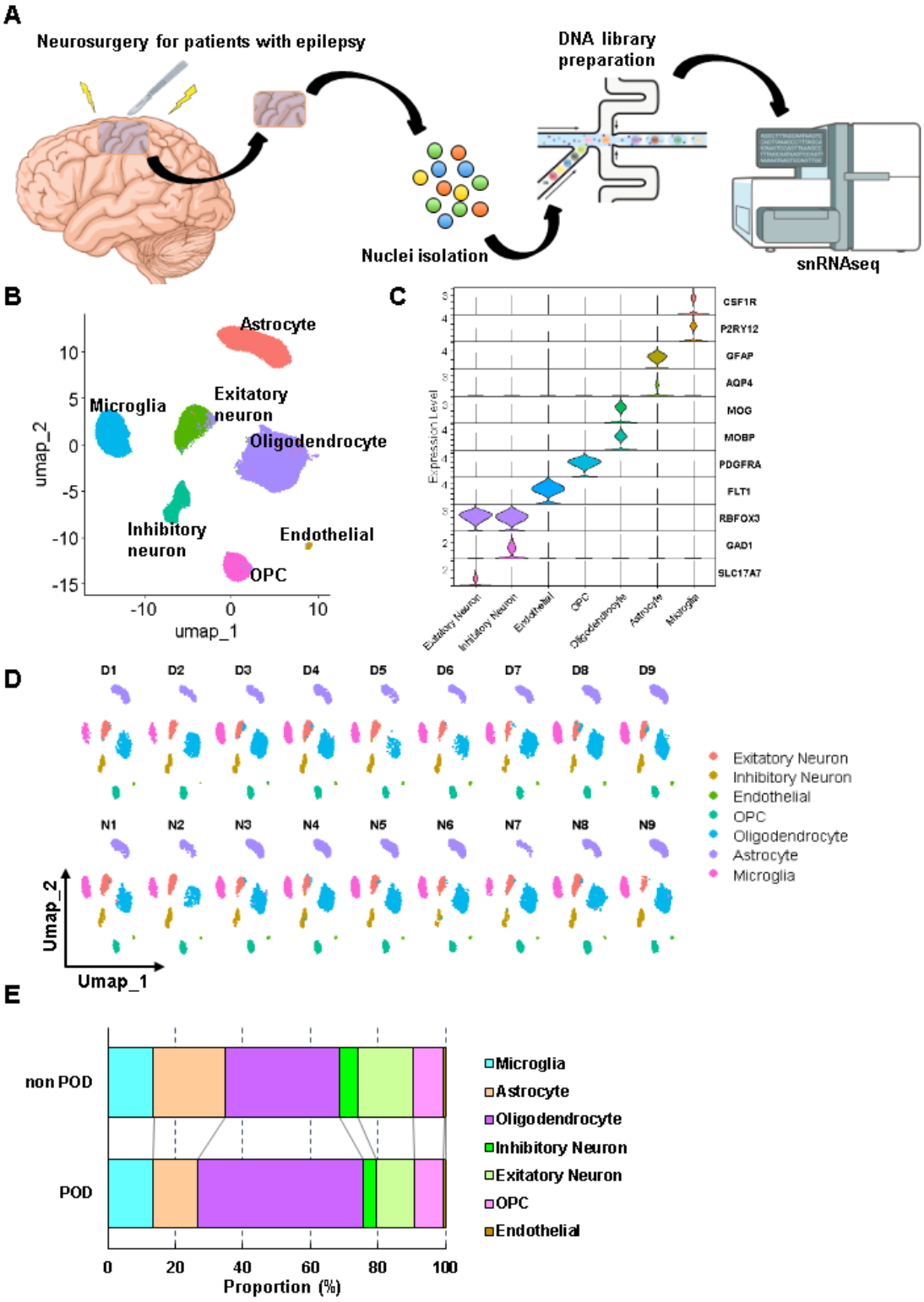

Figure 2. snRNAseq analysis for microglia cluster

A Research scheme for snRNAseq analysis using resected brain tissue

B UMAP for all nuclei colored by cell type annotations.

C Representative cell type specific marker genes expression

D UMAPs split by each sample.

E Proportions of each cell type

Figure 3

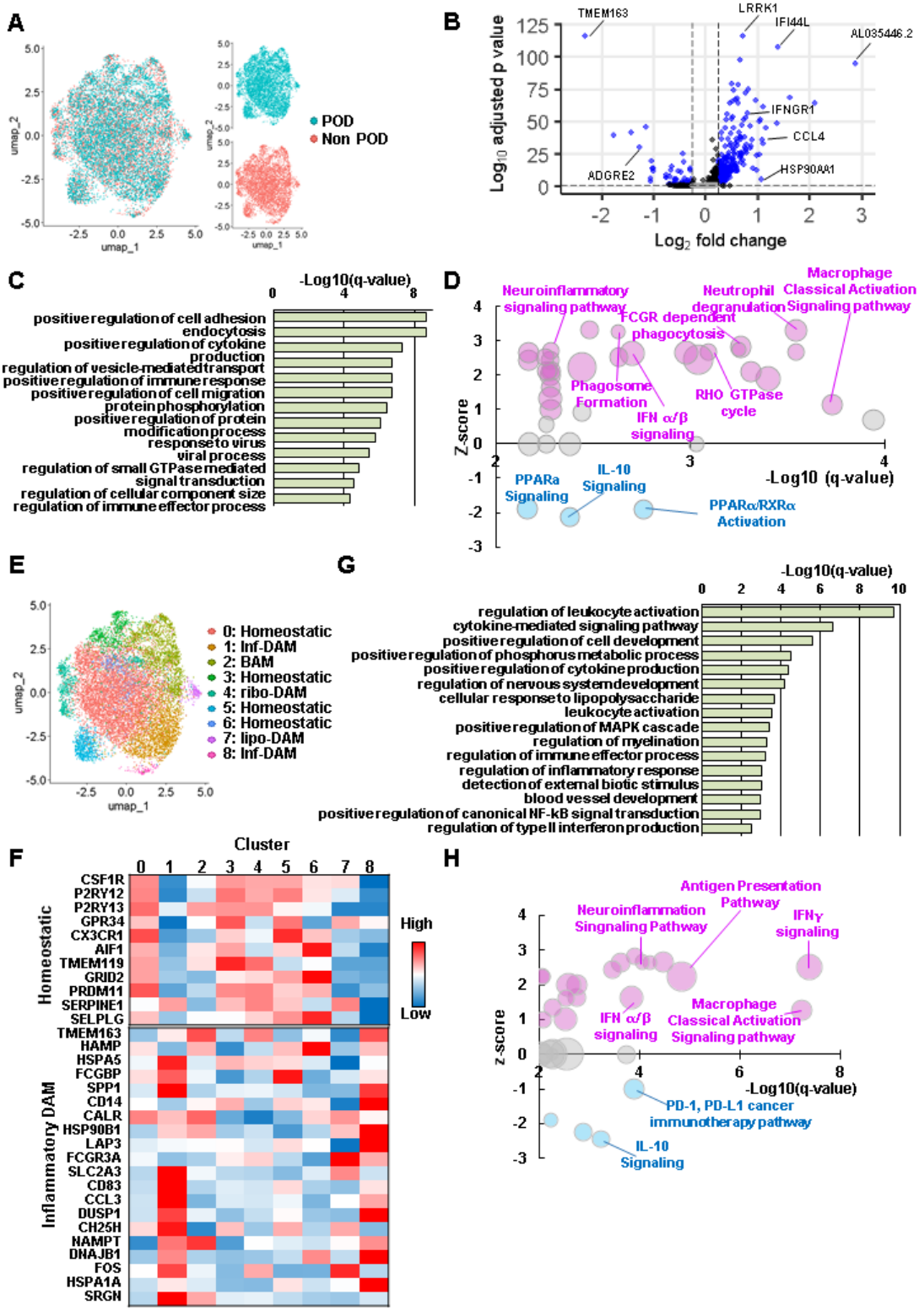

Figure 3. snRNAseq analysis for microglia cluster

A UMAP for microglia colored by the groups.

B DEGs described in volcano plot (non POD vs POD). Blue plots meet the criteria ($Log_2FC > 0.25$, adjusted p-value <0.05)

C Enriched GO bioprocess (BP) summary terms compared between non POD and POD groups.

D Enriched IPA pathways compared between non POD and POD groups (q-value<0.01). Bubble size means the ratio of DEGs/genes in the pathway (0.031-0.14). Magenta; activated (z-score ≥1), blue; inhibited (z-score ≤ -1), gray; random (|z-score| ≤ 1).

E UMAP for microglia colored by clusters.

F Relative gene expression level of representative homeostatic and inflammatory DAM markers .

G Enriched GO bioprocess (BP) summary terms for DAM cluster.

H Enriched IPA pathways for DAM cluster compared between non POD and POD groups (q-value<0.01). Bubble size means the ratio of DEGs/genes in the pathway (0.018 - 0.167). Magenta; activated (z-score ≥1), blue; inhibited (z-score ≤ -1), gray; random (|z-score| ≤ 1).

Figure 4

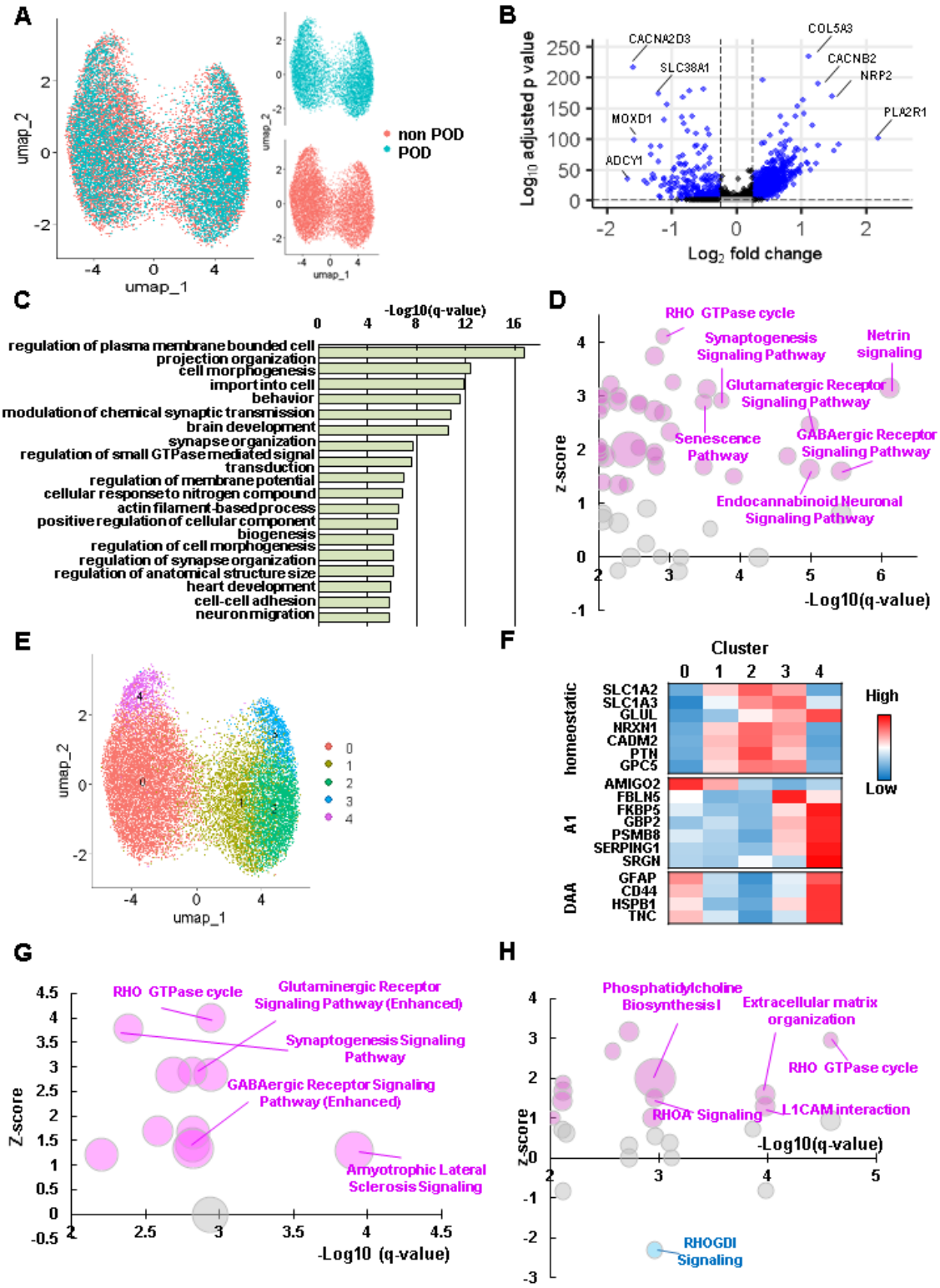

Figure 4. snRNAseq analysis for Astrocyte

A UMAP for all nuclei from astrocyte colored by groups

B DEGs described in volcano plot. Blue plots meet the criteria ($Log_2FC > 0.25$, adjusted p-value <0.05)

C Enriched GO bioprocess (BP) summary terms compared between non POD and POD groups.

D Enriched IPA pathways compared between non POD and POD groups (q-value<0.01). Bubble size means the ratio of DEGs/genes in the pathway (0.085-0.57). Magenta; activated (z-score ≥1), blue; inhibited (z-score ≤ -1), gray; random (|z-score| <1)

E UMAP for all nuclei from astrocyte colored by clusters

F Relative expression of representative markers in each astrocyte subcluster.

G Enriched IPA pathways for homeostatic astrocytes compared between non POD and POD groups (q-value<0.01). Bubble size means the ratio of DEGs/genes in the pathway (0.0867-0.176). Magenta; activated (z-score ≥1), blue; inhibited (z-score ≤ -1), gray; random (|z-score| <1)

H Enriched IPA pathways for activated astrocytes compared between non POD and POD groups (q-value<0.01). Bubble size means the ratio of DEGs/genes in the pathway (0.697-0.571). Magenta; activated (z-score ≥1), blue; inhibited (z-score ≤ -1), gray; random (|z-score| <1)

Figure 5

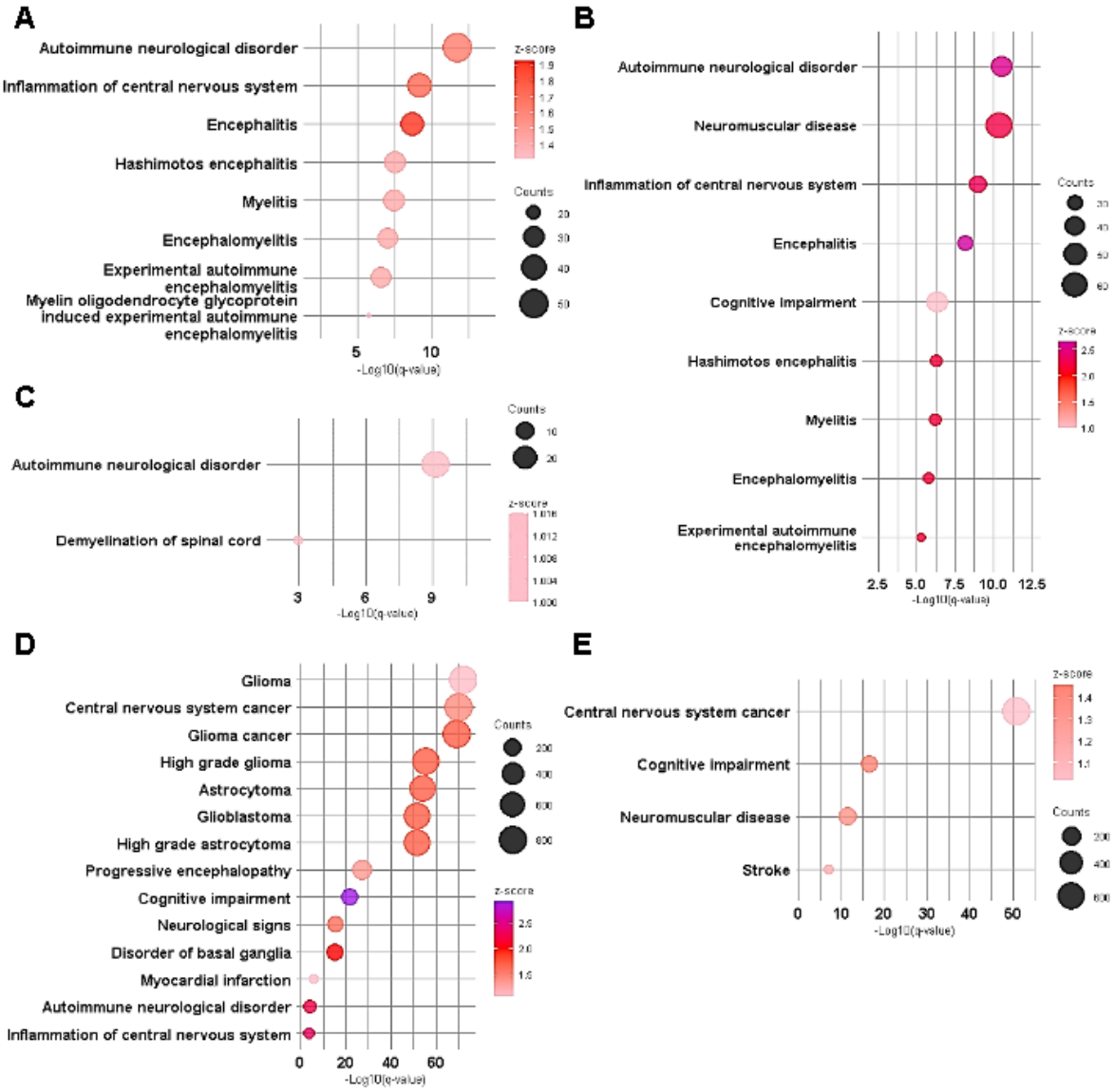

Figure 5. Downstream analysis for glial cells

A-E Enriched neurological-disease associated terms upregulated in POD group in whole microglia **(A),** homeostatic microglia **(B)**, inflammatory DAM **(C)**, whole astrocyte **(D)**, homeostatic astrocytes **(E)**. q-value <0.01. Bubble size means the gene counts of DEGs.

Figure S1

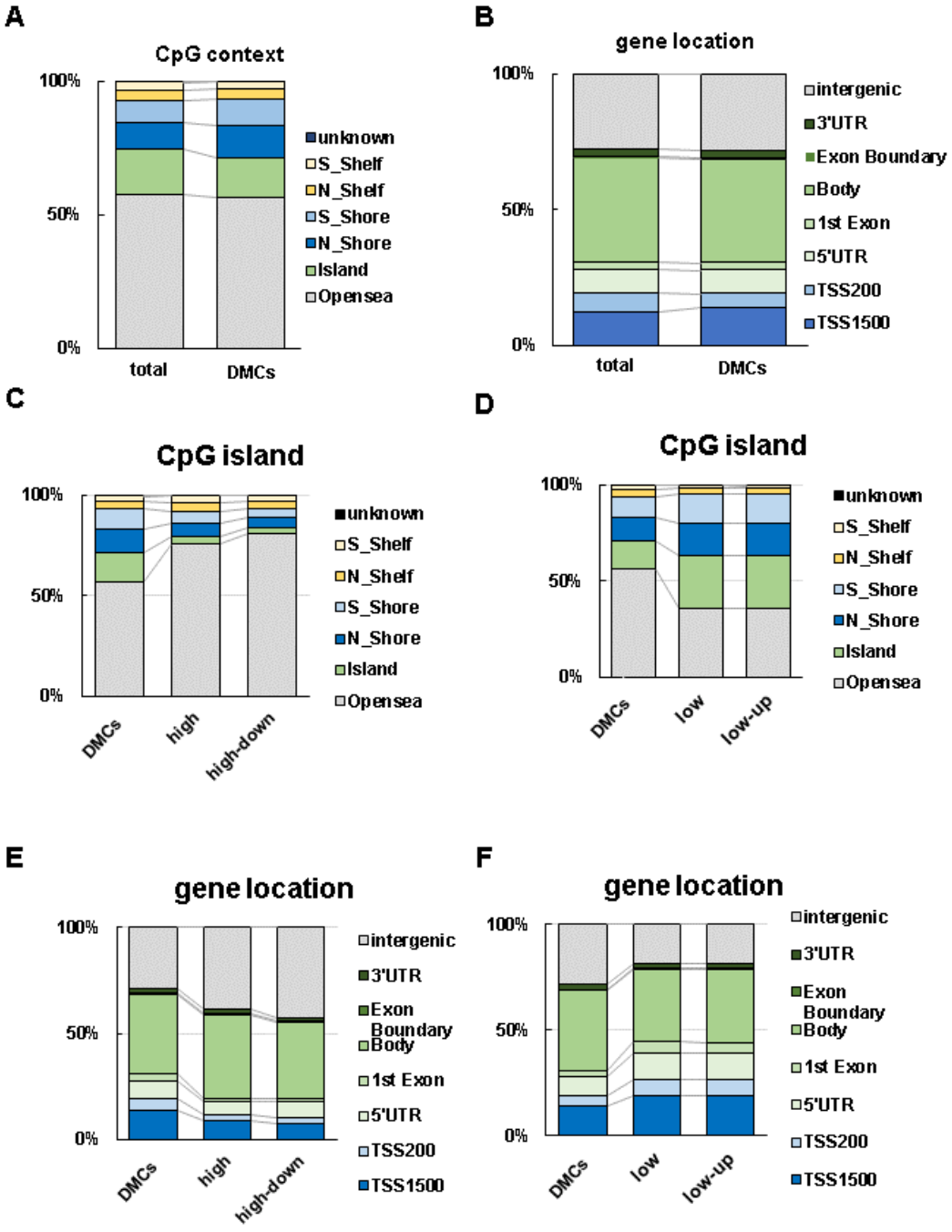

Figure S1. Characteristics of differentially methyrated CpGs

A, B the proportions of DMPs site location; A. CpG context and B. gene location.

C, D the detailed proportion of CpG context; C.high methylated DMPs D. low methylated DMPs

E, F the detailed proportion of gene location; E.high methylated DMPs F. low methylated DMPs

Figure S2

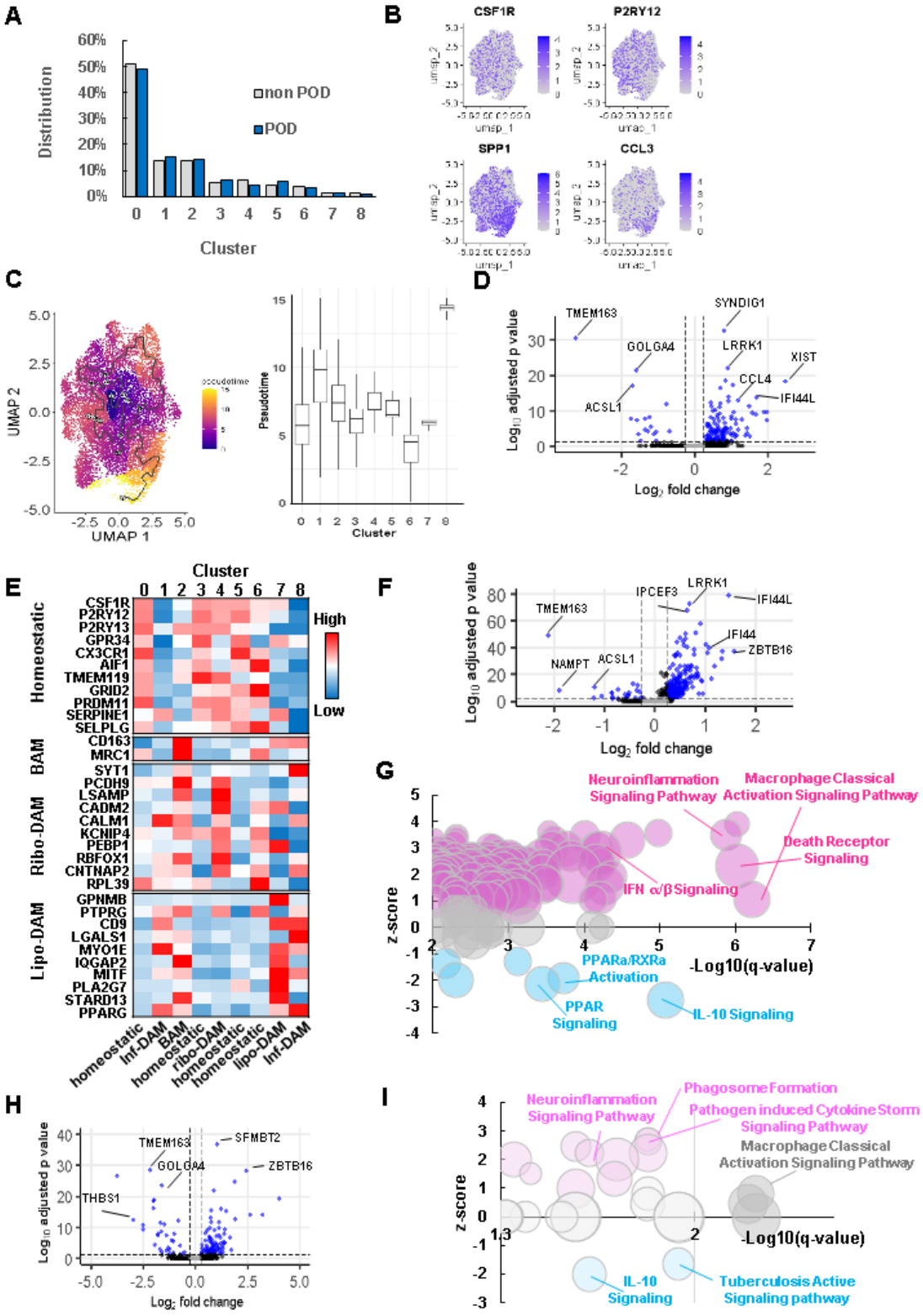

Figure S2. snRNAseq analysis for microglial sub-cluster

A Distribution of microglia in each sub-cluster

B Representative homeostatic and DAM marker expression

C Trajectory analysis for microglia cluster. pseudo time distribution in UMAP (left) and each cluster (right).

D DEGs in inflammatory DAM described in volcano plot. Blue plots meet the criteria ($Log_2FC > 0.25$, adjusted p-value <0.05)

E Gene expression level of representative homeostatic, BAM and DAM markers.

F DEGs in homeostatic microglia described in volcano plot. Blue plots meet the criteria ($Log_2FC > 0.25$, adjusted p-value <0.05)

G Enriched IPA pathways in homeostatic microglia cluster (q-value<0.01). Bubble size means the ratio of DEGs/genes in the pathway (0.0271- 0.208). Magenta; activated (z-score ≥1), blue; inhibited (z-score ≤ -1) , gray; random (|z-score| ≤ 1) .

H DEGs in BAM described in volcano plot. Blue plots meet the criteria ($Log_2FC > 0.25$, adjusted p-value <0.05)

I Enriched IPA pathways in BAM cluster compared between non POD and POD groups (q-value<0.01). Bubble size means the ratio of DEGs/genes in the pathway (0.0128- 0.0727). Magenta; activated (z-score ≥1), blue; inhibited (z-score ≤ -1), gray; random (|z-score| ≤ 1).

Figure S3

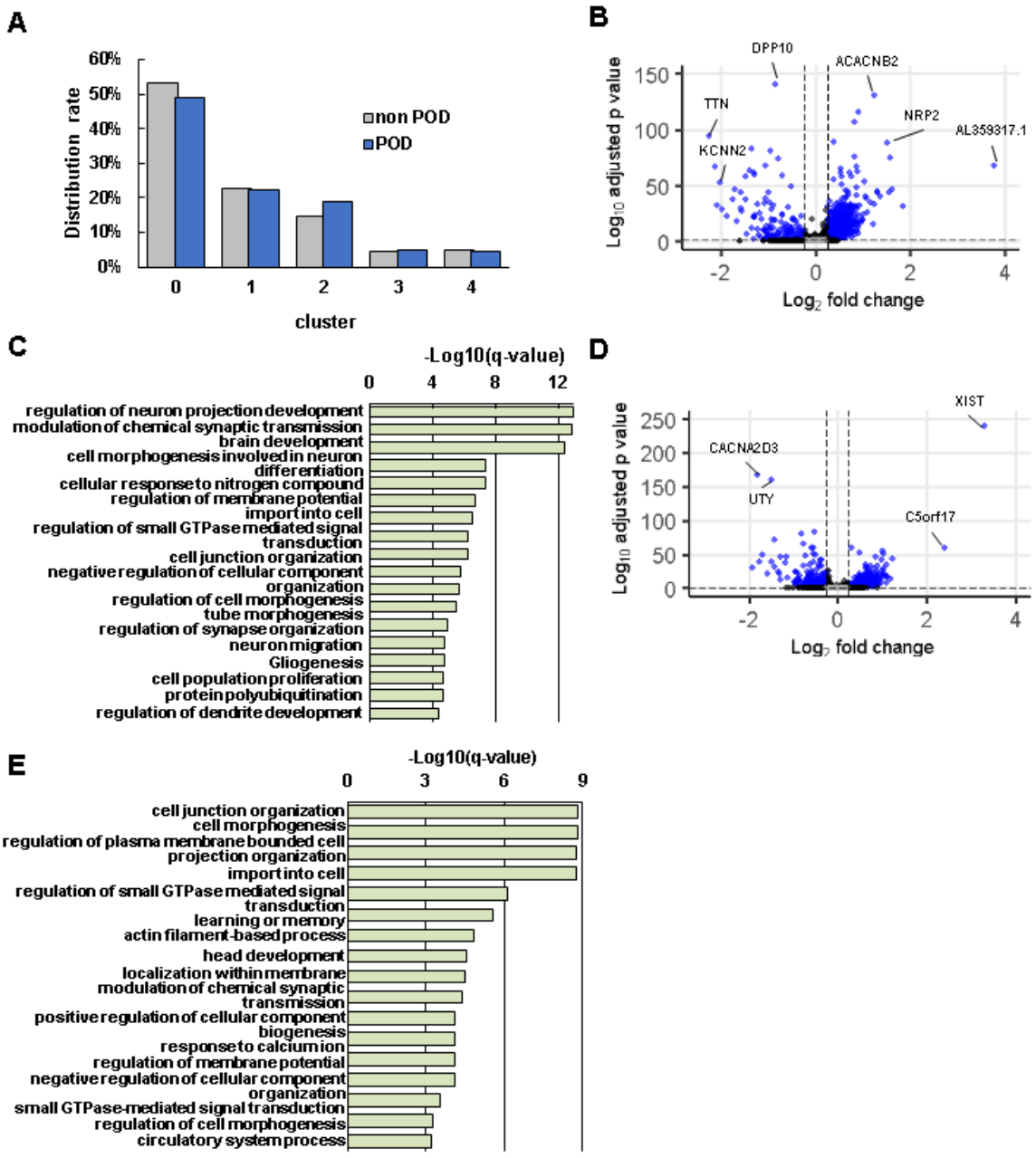

Figure S3. snRNAseq analysis for astrocyte sub-cluster

A Distribution of astrocyte in each sub-cluster

B DEGs in basic astrocyte cluster described in volcano plot. Blue plots meet the criteria (Log_2FC > 0.25, adjusted p-value <0.05)

C Enriched GO bioprocess (BP) summary terms in homeostatic astrocytes

D DEGs in activated astrocyte cluster described in volcano plot. Blue plots meet the criteria ($Log_2FC > 0.25$, adjusted p-value <0.05)

E Enriched GO bioprocess (BP) summary terms in activated astrocytes

F Relative expression of representative markers in each astrocyte subcluster

Figure S4

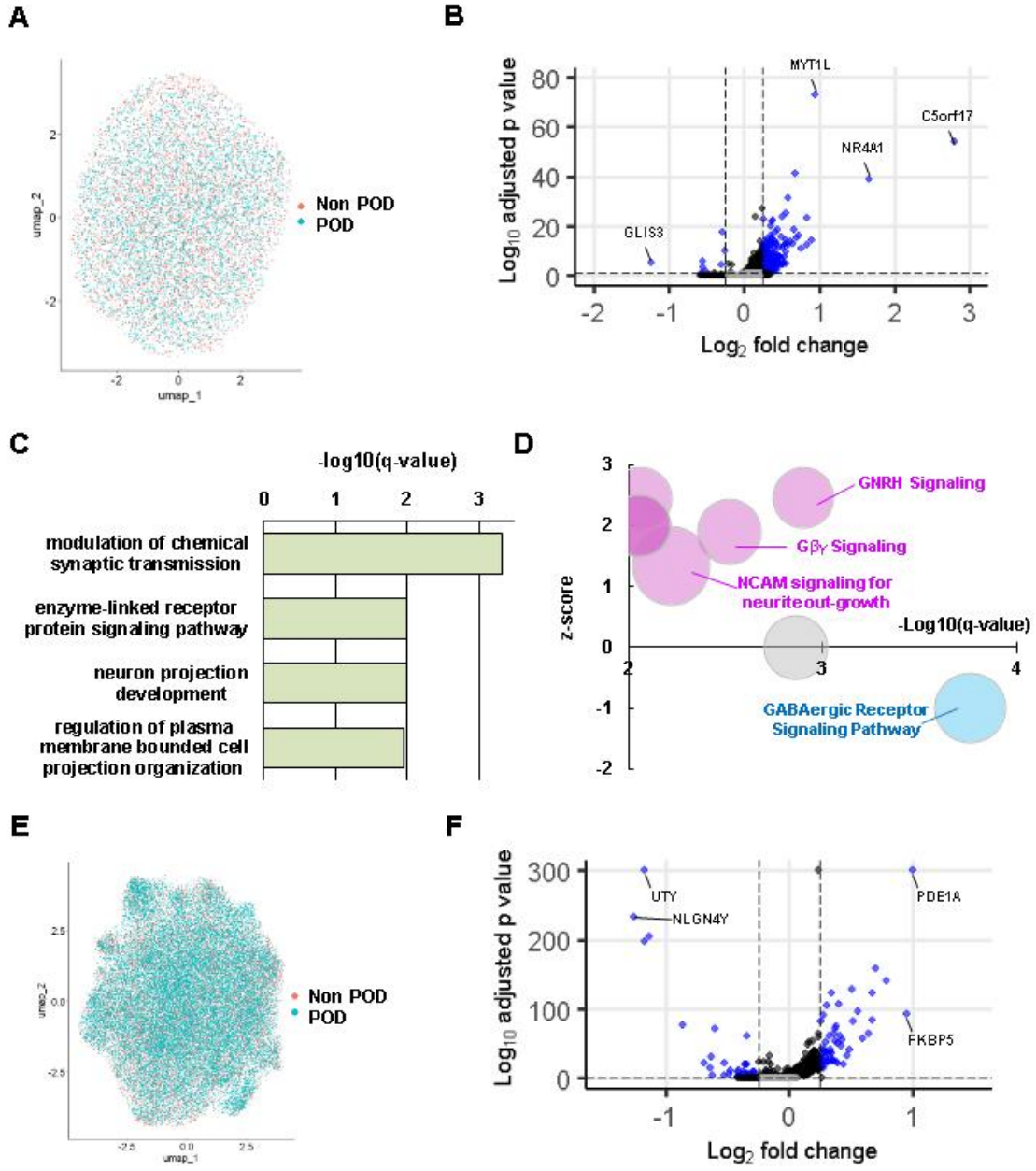

Figure S4. snRNAseq analysis for OPC and Oligodendrocyte cluster

A UMAP for all nuclei from OPCs colored by groups

B DEGs in OPCs described in volcano plot. Blue plots meet the criteria ($Log_2FC > 0.25$, adjusted p-value <0.05)

C Enriched GO bioprocess (BP) summary terms in OPCs

D Enriched IPA pathways in OPCs (q-value<0.01). Bubble size means the ratio of DEGs/genes in the pathway (0.0412-0.0794). Magenta; activated (z-score ≥1), blue; inhibited (z-score ≤ -1), gray; random (|z-score| < 1)

E UMAP for all nuclei from oligodendrocyte colored by groups

F DEGs described in volcano plot. Blue plots meet the criteria ($Log_2FC > 0.25$, adjusted p-value <0.05)

Figure S5

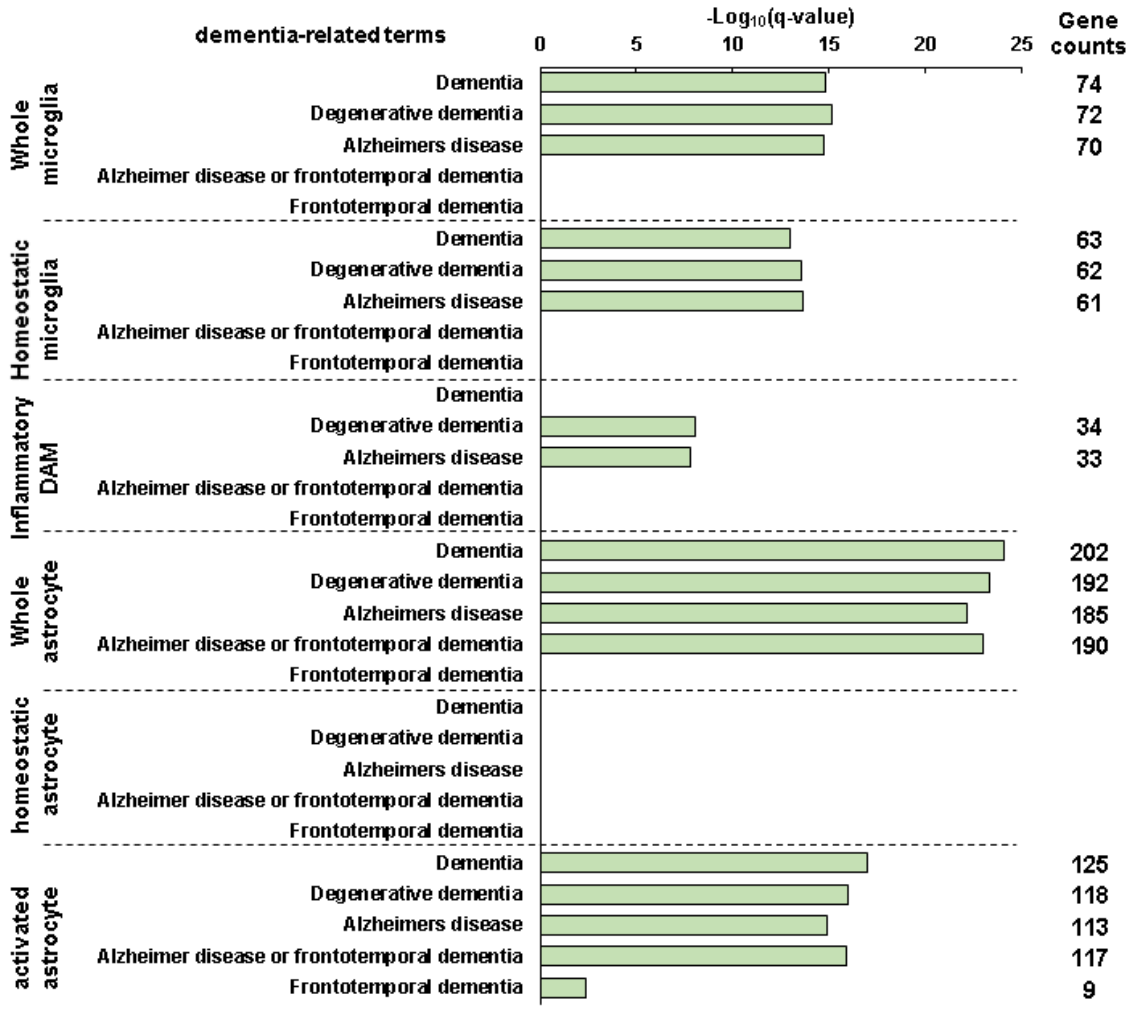

Figure S5. Dementia-related terms in microglia and astrocytes

Statistical significance of 5 dementia-related terms in microglia and astrocytes clusters.